Computer Physics Communications 278 (2022) 108403

Contents lists available at ScienceDirect

Computer Physics Communications

www.elsevier.com/locate/cpc

Relativistic radial electron density functions and natural orbitals from GRASP2018 ☆,☆☆

S. Schiffmann [a,b], J.G. Li [c], J. Ekman [d], G. Gaigalas [e], M. Godefroid [a], P. Jönsson [d], J. Bieroń [f]

[a] Spectroscopy, Quantum Chemistry and Atmospheric Remote Sensing, Université libre de Bruxelles, Brussels, Belgium
[b] Division of Mathematical Physics, Department of Physics, Lund University, SE-22100 Lund, Sweden
[c] Institute of Applied Physics and Computational Mathematics, 100088 Beijing, People's Republic of China
[d] Department of Materials Science and Applied Mathematics, Malmö University, SE-20506 Malmö, Sweden
[e] Institute of Theoretical Physics and Astronomy, Vilnius University LT-010222 Vilnius, Lithuania
[f] Instytut Fizyki Teoretycznej, Uniwersytet Jagielloński, Kraków, Poland

ARTICLE INFO

Article history:
Received 8 June 2021
Received in revised form 14 April 2022
Accepted 2 May 2022
Available online 10 May 2022

Keywords:
Electron density
Density matrix
Natural orbitals
Multiconfiguration wave functions
Relativistic contraction

ABSTRACT

A new module, RDENSITY, of the GRASP2018 package [1] is presented for evaluating the radial electron density function of an atomic state described by a multiconfiguration Dirac-Hartree-Fock or configuration interaction wave function in the fully relativistic scheme. The present module is the relativistic version of DENSITY [2] that was developed for the ATSP2K package [3]. The calculation of the spin-angular factors entering in the expression of the expectation value of the density operator is performed using the angular momentum theory in orbital, spin, and quasispin spaces, adopting a generalized graphical technique [4]. The natural orbitals (NOs) are evaluated from the diagonalization of the density matrix, taking advantage of its κ-block structure. The features of the code are discussed in detail, focusing on the advantages and properties of the NOs and on the electron radial density picture as a mean for investigating electron correlation and relativistic effects.

Program summary

Program title: RDENSITY
CPC Library link to program files: https://doi.org/10.17632/4sdrf5kfzd.1
Licensing provisions: MIT license
Programming language: FORTRAN 95
Nature of problem: This program determines the atomic electron radial density in the MCDHF approximation. It also evaluates the natural orbitals by diagonalizing the density matrix.
Solution method: Building the density operator using second quantization - Spherical symmetry averaging - Evaluating the matrix elements of the one-body excitation operators in the configuration state function (CSF) space using the angular momentum theory in orbital, spin, and quasispin spaces.
Additional comments including restrictions and unusual features: We evaluated the electron radial density and natural orbitals of the lowest states in Mg II. The MCDHF wave functions consisted of four non-interacting blocks and a total of 79 000 CSFs. The calculation took around 2 minutes using a computer with an Intel(R) Xeon(R) Gold 6148 processor @ 2.4 GHz.

References

[1] GRASP2018 - A Fortran 95 version of the General Relativistic Atomic Structure Package, C. Froese Fischer, G. Gaigalas, P. Jönsson and J. Bieroń, Comput. Phys. Commun. **237** (2019) 184-187.
[2] Multiconfiguration electron density function for the ATSP2K-package, A. Borgoo, O. Scharf, G. Gaigalas and M. Godefroid, Comput. Phys. Commun. **181** (2010) 426-439
[3] An MCHF atomic-structure package for large-scale calculations, C. Froese Fischer, G. Tachiev, G. Gaigalas, and M. Godefroid, Comput. Phys. Commun. **176** (2007) 559-579

☆ The review of this paper was arranged by Prof. N.S. Scott.
☆☆ This paper and its associated computer program are available via the Computer Physics Communications homepage on ScienceDirect (http://www.sciencedirect.com/science/journal/00104655).

E-mail addresses: saschiff@ulb.ac.be (S. Schiffmann), mrgodef@ulb.ac.be (M. Godefroid).

https://doi.org/10.1016/j.cpc.2022.108403

[4] An efficient approach for spin-angular integrations in atomic structure calculations, G. Gaigalas, Z. Rudzikas, and C. Froese Fischer, J. Phys. B: At. Mol. Phys., **30** (1997) 3747-3771

1. Introduction

The electron density function and the natural orbitals are derived from the one-dimensional (spin)-density matrices as introduced by Löwdin [1]. Although natural orbitals were successfully used in quantum chemistry [2–4] and in atomic physics [5–7], they are mostly known for their compactness properties [8], especially for two-electron expansions [9,10]. It is worthwhile to mention that there is a whole field of one-body reduced density matrix functional theory in which NOs play a role similar to Kohn-Sham/Hartree-Fock (KS/HF) orbitals (see for instance [11–13]). Recent efforts were made to re-investigate the use of natural orbitals in coupled-electron pair approaches [14] and their usefulness for multiconfiguration expansions [15]. The non-relativistic `DENSITY` program [16] computes the electron radial density and the natural orbitals in the framework of the non-relativistic multiconfiguration Hartree-Fock (MCHF) method. Its applications focused almost exclusively on the use of the radial density function [17,16] and only presented the natural orbitals in nominal two electron systems, e.g., generating the natural expansion $1s^2nl^2\ {}^1S$ of the valence correlation multiconfiguration expansion of the Be ground state. Properties of the natural orbitals in many-electron atomic systems are still poorly known as attests the recent paper on the hyperfine structure of sodium using natural orbitals [18], which gives a glimpse of their potential in relativistic multiconfiguration calculations [19].

Besides the application to natural orbitals, the present program provides the electron radial density, which is an interesting tool to probe electronic structures. Recently, the electron radial density of the $_{118}$Og ground state was computed [20], confirming the results obtained with electron localization functions [22]. The comparison of non-relativistic and relativistic electron densities demonstrates a significant change in behaviour of the outer valence shells due to relativistic effects, which could lead to unexpected chemical properties of the heaviest noble gas [21,22].

2. The spherical electron density function

The present approach is limited to the description of field-free atoms. In analogy with the non-relativistic framework [16], a spherical electron density function, independent of the polar and azimuthal angles, $\rho(r)$, can be obtained for an atomic state $|\alpha J\rangle$ by averaging the $2J+1$ density functions $\rho(\mathbf{r})^{\alpha JM_J}$

$$\rho(\mathbf{r})^{\alpha J} \equiv \frac{1}{(2J+1)} \sum_{M_J} \rho(\mathbf{r})^{\alpha JM_J} \,, \tag{1}$$

evaluated at point $\mathbf{r}(x, y, z)$ and constructed according to

$$\rho(\mathbf{r})^{\alpha JM_J} = \sum_{pq} \langle \Psi_{\alpha JM_J} | a_p^\dagger a_q | \Psi_{\alpha JM_J} \rangle \ \psi_p^\dagger(\mathbf{r}) \psi_q(\mathbf{r}) \tag{2}$$

for each magnetic component $-J \le M_J \le +J$ of the atomic state wave function $\Psi_{\alpha JM_J}$. The latter is written as an expansion of relativistic configuration state functions (CSFs)

$$\Psi_{\alpha JM_J} = \sum_{i=1}^{N_{\rm CSFs}} c_i \, \Phi(\alpha_i JM_J) \,, \tag{3}$$

where α represents the complete set of configuration and coupling tree quantum numbers that uniquely specify the considered atomic state in the JM_J symmetry subspace. Expressing the CSFs $\{\Phi(\alpha_i JM_J)\}$ in terms of normalized N-electron determinant product states, i.e. Slater determinants, the operators a_k and $a_k^\dagger$ annihilate and create respectively an electron described by the one-electron Dirac spinor

$$\psi_k(\mathbf{r}) = \langle \mathbf{r} | a_k^\dagger | 0 \rangle = \frac{1}{r} \begin{pmatrix} P_{n\kappa}(r) \chi_{\kappa m_j}(\theta, \phi) \\ \mathrm{i} Q_{n\kappa}(r) \chi_{-\kappa m_j}(\theta, \phi) \end{pmatrix} \,, \tag{4}$$

where k is the shorthand notation for four quantum numbers $k = (n, l, j, m_j) = (n, \kappa, m_j)$. κ implicitly contains the (l, j) quantum numbers through the relation $\kappa = (2j+1)(l-j)$, i.e. $\kappa = -(l+1)$ for $j = l + 1/2$, and $\kappa = +l$ for $j = l - 1/2$. $P_{n\kappa}(r)$ and $Q_{n\kappa}(r)$ are the radial functions of the large and small components, respectively, that are determined by solving numerically the MCDHF radial equations[1] while $\chi_{\kappa m_j}$ are two-component spherical spinors (see [19,24]).

Defining the radial density operator as

$$\delta(r) \equiv \sum_{i=1}^{N} \delta(r - r_i) \,, \tag{5}$$

[1] Note that there is no need to refer to the no-pair approximation [23] in GRASP since the negative energy states appeared to have no influence on the finite difference methods of (MC)DHF codes - essentially because each positive energy spinor is the solution of a single inhomogeneous Dirac equation with well-posed boundary conditions and interaction terms that change from one self-consistent iteration to the next. In other terms, there are no pairs because the negative energy states are just ignored.

the associated second quantization operator is

$$\hat{\delta}(r) = \sum_{pq} d_{pq}(r)\, a_p^\dagger a_q \,, \tag{6}$$

with

$$d_{pq}(r) = \delta_{l_p l_q}\, \delta_{j_p j_q}\, \delta_{m_{j_p} m_{j_q}} \left[P^*_{n_p\kappa_p}(r) P_{n_q\kappa_q}(r) + Q^*_{n_p\kappa_p}(r) Q_{n_q\kappa_q}(r) \right] , \tag{7}$$

where the Kronecker delta arises from the orthonormality property of one-electron Dirac spinors. Assuming *real* radial one-electron functions, and using $\delta_{l'l}\, \delta_{j'j} = \delta_{\kappa'\kappa}$, the operator (6) becomes

$$\hat{\delta}(r) = \sum_{n',l',j',m'_j,n,l,j,m_j} \delta_{l'l}\, \delta_{j'j}\, \delta_{m'_j m_j}\, a^\dagger_{n'l'j'm'_j} a_{nljm_j} \, [P_{n'\kappa'}(r) P_{n\kappa}(r) + Q_{n'\kappa'}(r) Q_{n\kappa}(r)] \tag{8}$$

$$= \sum_{n',n} \sum_{l,j,m_j} a^\dagger_{n'ljm_j} a_{nljm_j} \, [P_{n'\kappa}(r) P_{n\kappa}(r) + Q_{n'\kappa}(r) Q_{n\kappa}(r)] \,. \tag{9}$$

Its expectation value provides the radial density distribution $D(r) \equiv 4\pi r^2 \rho(r)$. Building the irreducible tensor of rank zero from the $(2j+1)$ components of the creation and annihilation operators [25,26]

$$\left(\mathbf{a}^\dagger_{n'lj}\, \mathbf{a}_{nlj} \right)^{(0)}_0 = -\frac{1}{\sqrt{2j+1}} \sum_{m_j} a^\dagger_{n'ljm_j} a_{nljm_j} \,, \tag{10}$$

the operator (8) becomes

$$\hat{\delta}(r) = \hat{\delta}(r)^{(0)}_0 = -\sum_j \sqrt{2j+1} \sum_{n,\, n',\, l} \left(\mathbf{a}^\dagger_{n'lj}\, \mathbf{a}_{nlj} \right)^{(0)}_0 I_\rho \left(n'\kappa, n\kappa; r \right) \,, \tag{11}$$

with

$$I_\rho \left(n'\kappa, n\kappa; r \right) \equiv \left[P_{n'\kappa}(r) P_{n\kappa}(r) + Q_{n'\kappa}(r) Q_{n\kappa}(r) \right] . \tag{12}$$

The expectation value of this operator provides the radial electron density distribution for any atomic state $\Psi_{\alpha JM}$. Using the Edmonds/Racah [27] version of the Wigner-Eckart theorem, the radial density $D(r) = 4\pi r^2 \rho(r)$ can be calculated from the expectation value of the one-particle scalar operator (11),

$$\langle \Psi_{\alpha J M_J} | \hat{\delta}(r)^{(0)}_0 | \Psi_{\alpha J M_J} \rangle = (-1)^{J-M_J} \begin{pmatrix} J & 0 & J \\ -M_J & 0 & M_J \end{pmatrix} \langle \Psi_{\alpha J} \| \hat{\delta}(r)^{(0)} \| \Psi_{\alpha J} \rangle \,. \tag{13}$$

From the analogy of the operator (11) and the relativistic one-body Dirac Hamiltonian operator, one deduces that the spin-angular coefficients $v^{ij}_{n'n\kappa}$ of the radial functions $I_\rho \left(n'\kappa, n\kappa; r \right)$ appearing in the matrix element $\langle \Phi(\alpha_i J M_J) | \hat{\delta}(r) | \Phi(\alpha_j J M_J) \rangle$ are identical to those of the one-electron Hamiltonian radial integrals $I_{n'\kappa, n\kappa}$ in the Hamiltonian matrix. This was already observed in the context of biorthonormal orbital transformation in the non-relativistic framework (see eq. (A5) of [28]) and is fully consistent with the analysis of McWeeny [29] for determinantal molecular wave functions.

Combining the second quantization and quasispin methods with the theory of angular momentum and irreducible tensor operators [30], the spin-angular coefficients $v^{ij}_{n'n\kappa}$, also denoted as $t^0_{ij}(n'n\kappa)$ in [31], can be derived by working out the reduced matrix elements of the one–particle scalar operator $\widehat{F}^{(0)}$ between configuration state functions, $\Phi(\alpha_i J)$ and $\Phi(\alpha_j J)$. Gaigalas et al. [31] expressed the latter as a sum over one–electron contributions

$$\begin{aligned} \langle \Phi(\alpha J) \left\| \widehat{F}^{(0)} \right\| \Phi(\alpha' J) \rangle &= \sum_{n_p l_p j_p, n_q l_q j_q} \langle \Phi(\alpha J) \left\| \widehat{F}(n_p l_p j_p, n_q l_q j_q) \right\| \Phi(\alpha' J) \rangle \\ &= \sum_{n_p\kappa_p, n_q\kappa_q} \langle \Phi(\alpha J) \left\| \widehat{F}(n_p\kappa_p, n_q\kappa_q) \right\| \Phi(\alpha' J) \rangle \,, \end{aligned} \tag{14}$$

where

$$\begin{aligned} \langle \Phi(\alpha J) \left\| \widehat{F}(n_p\kappa_p, n_q\kappa_q) \right\| \Phi(\alpha' J) \rangle &= (-1)^{\Delta+1} \sqrt{2j_p+1}\, R \left(j_p, j_q, \Lambda^{bra}, \Lambda^{ket} \right) \delta(\kappa_p, \kappa_q) \left(n_p\kappa_p \left\| f^{(0)} \right\| n_q\kappa_q \right) \\ &\times \left\{ \delta(n_p, n_q) \left(j_p^{N_p}\, \alpha_p Q_p J_p \left\| \left[a^{(q\ j_p)}_{1/2} \times a^{(q\ j_p)}_{-1/2} \right]^{(0)} \right\| j_p^{N_p}\, \alpha_p Q_p J_p \right) \right. \\ &+ (1 - \delta(n_p, n_q)) \left(j_p^{N_p}\, \alpha_p Q_p J_p \left\| a^{(q\, j_p)}_{1/2} \right\| j_p^{N'_p}\, \alpha_p Q_p J_p \right) \left. \left(j_q^{N_q}\, \alpha_q Q_q J_q \left\| a^{(q\, j_q)}_{-1/2} \right\| j_q^{N'_q}\, \alpha_q Q_q J_q \right) \right\} . \end{aligned} \tag{15}$$

In these expressions, all states are defined in jj–coupling. Details of the underlying Racah-Wigner machinery and algebra combining second quantization and quasi-spin representation of states can be found in [32,33]. R is a recoupling matrix [34], $\Lambda^{bra} \equiv \left(J_p, J_q, J_{p'}, J_{q'} \right)^{bra}$ and $\Lambda^{ket} \equiv \left(J_p, J_q, J_{p'}, J_{q'} \right)^{ket}$ denote the respective sets of active subshell angular momenta, and $\left(n_p\kappa_p \left\| f^{(0)} \right\| n_q\kappa_q \right)$ is the one–electron

reduced matrix element of the operator $\widehat{F}^{(0)}$. The operators $a^{(q\,j)}_{m_q}$ are second quantization operators in quasispin space of rank $q = 1/2$. Adopting the Vilnius school convention [30], the operator $a^{(q\,j)}_{1/2\,m_j} = a^{(j)}_{m_j}$ creates electrons with angular momentum quantum numbers j, m_j and its conjugate $a^{(q\,j)}_{-1/2\,m_j} = \tilde{a}^{(j)}_{m_j} = (-1)^{j-m_j} a^{(j)+}_{-m_j}$ annihilates electrons with the same quantum numbers j, m_j in a given subshell. The pure spin-angular coefficients for scalar one-electron operators in the CSFs basis can be identified by inserting

$$\left(n_i\kappa_i \left\| f^{(0)} \right\| n_j\kappa_j\right) = 1 \tag{16}$$

in (14). Just like the one-electron matrix elements of the Dirac operator, another tensor operator of rank zero,

$$\left(n_i\kappa_i \left\| \widehat{H}_D \right\| n_j\kappa_j\right) = I(n_i l_i j_i, n_j l_i j_i)\, \delta(\kappa_i, \kappa_j)\ , \tag{17}$$

one has for the radial density

$$\left(n_i\kappa_i \left\| \hat{\delta}(r) \right\| n_j\kappa_j\right) = I_\rho(n_i l_i j_i, n_j l_i j_i; r)\, \delta(\kappa_i, \kappa_j) = I_\rho(n_i\kappa_i, n_j\kappa_i; r)\, \delta(\kappa_i, \kappa_j)\ . \tag{18}$$

3. Density matrix and natural orbitals

Using (3), and (13)–(15), the radial density distribution becomes

$$D(r) = 4\pi r^2 \rho(r) = \sum_{ij} c_i^*\, D_{ij}(r)\, c_j = \sum_{ij} c_i^* \left[\sum_\kappa \sum_{n'n} v^{ij}_{nn'\kappa}\, I_\rho(n'\kappa, n\kappa; r) \right] c_j\ , \tag{19}$$

where $\{c_i\}$ are the CSF mixing coefficients appearing in the atomic state function (3), $\{c_i^*\}$ their complex conjugate, and where $v^{ij}_{nn'\kappa}$ are the spin-angular coefficients introduced in previous section. It can be rewritten in the following compact form

$$D(r) = \sum_\kappa \sum_{n'n} \rho^\kappa_{n'n}\, I_\rho(n'\kappa, n\kappa; r)\ , \tag{20}$$

with

$$\rho^\kappa_{n'n} = \sum_{ij} c_i^*\, v^{ij}_{nn'\kappa}\, c_j\ . \tag{21}$$

The $\delta(\kappa_p, \kappa_q)$ Kronecker appearing in (15) assures the block-structure of the density matrix $\boldsymbol{\rho}$ whose elements are defined by (21) for the κ-symmetry.

The natural orbitals (NO) are defined as the one-electron functions that diagonalize the density matrix $\boldsymbol{\rho}$

$$\mathbf{C}^\dagger \boldsymbol{\rho}\, \mathbf{C} = \widetilde{\boldsymbol{\rho}}\ . \tag{22}$$

Within a specific κ-symmetry, the eigenvalue problem for the relevant κ-block

$$\boldsymbol{\rho}^\kappa\, \mathbf{C}^\kappa = \mathbf{C}^\kappa\, \widetilde{\boldsymbol{\rho}}^\kappa\ , \tag{23}$$

defines the natural radial orbitals through the following transformation

$$\begin{cases} \widetilde{P}_{\alpha\kappa}(r) &= \sum_n c^\kappa_{n,\alpha} P_{n\kappa}(r) \\ \widetilde{Q}_{\alpha\kappa}(r) &= \sum_n c^\kappa_{n,\alpha} Q_{n\kappa}(r)\ . \end{cases} \tag{24}$$

The eigenvalues $\{\lambda_i^\kappa \equiv \tilde{\rho}_{ii}^\kappa\}$ are interpreted as the occupation numbers of the NOs $\left\{\left(\widetilde{P}_{\alpha\kappa}(r), \widetilde{Q}_{\alpha\kappa}(r)\right)\right\}$.

4. Program description

4.1. File naming conventions

The `RDENSITY` program is compatible with the GRASP package [35,36] and therefore relies on its data storage system. As already described for the relativistic isotope shift `RIS4` program [37], data within GRASP are passed through the use of files. External programs such as `RDENSITY` must therefore be able to read and write data in the correct format, e.g., radial wave functions, mixing coefficients or CSFs lists. External programs should also adhere to the GRASP input and output file name convention as described in its manual [38] and in the `RIS4` publication [37]. The present program outputs the radial density distribution and function, $D(r)$ and $\rho(r) = D(r)/(4\pi r^2)$, respectively, on the `<name>.d` formatted file. The natural orbitals (24) are written on the binary file `<name>.nw`.

```
Eigenvectors after reordering according to decreasing eigenvalues:
            #1          #2          #3          #4          #5
   1s  -0.9962701   0.0862396  -0.0008759  -0.0027906   0.0000442
   2s   0.0783755   0.8903450  -0.0764105  -0.4419319   0.0008265
   3s   0.0296733   0.3647526  -0.4200230   0.8130559   0.1691030
   4s   0.0170433   0.2137402   0.5445812   0.3381006  -0.7369830
   5s   0.0114944   0.1453242   0.7219229   0.1712209   0.6544154
Eigenvectors after reordering according to dominance:
   1s  -0.9962701   0.0862396  -0.0027906   0.0000442  -0.0008759
   2s   0.0783755   0.8903450  -0.4419319   0.0008265  -0.0764105
   3s   0.0296733   0.3647526   0.8130559   0.1691030  -0.4200230
   4s   0.0170433   0.2137402   0.3381006  -0.7369830   0.5445812
   5s   0.0114944   0.1453242   0.1712209   0.6544154   0.7219229
```

Fig. 1. Eigenvector compositions of natural orbitals corresponding to the $nsn's\ ^1S_0$ $n' \leq n = 1, \ldots, 5$ CSFs expansion of the He ground state. Each column corresponds to an eigenvector, initially in decreasing order of their corresponding eigenvalues and, finally, sorted according to dominance. (For interpretation of the colours in the figure(s), the reader is referred to the web version of this article.)

4.2. The algorithm

The algorithm in `RDENSITY` follows closely the one implemented in its non-relativistic counterpart `DENSITY` [16]. An obvious difference is that the density matrices (21) are built for each κ-symmetry instead of l-symmetry in the non-relativistic case. Most of the subroutines are taken from the `RIS4` program, in which the radial density at the nucleus is computed to evaluate the field shift [37]. The reader is referred to this work for details on the nuclear models implemented in GRASP. Among the new routines, `rdensity` governs the entire calculations, mostly setting up all parameters and calling GRASP libraries. Its call to `rdensity_cal` starts the calculations of the relativistic density. The core of the calculations is performed by the `natorbnew` subroutine. The density matrices (21) are computed, requiring to call the angular `ONESCALAR` routine available in GRASP libraries. The radial densities, for each κ, are accumulated by sweeping over the left and right hand CSF expansions in Eq. (13). Then, the density matrices are diagonalized using the LAPACK `dsyev` routine [39]. Finally, their corresponding eigenvectors are used to build the natural orbitals as linear combinations of the original orbital basis.

The novelty compared to the non-relativistic density program is that the labelling of the constructed natural orbitals is left to the user. Two options are available

1. according to the dominant component,
2. according to the decreasing order of the eigenvalues of the density matrices.

As an example, let us consider the He ground state CSFs expansion, $nsn's\ ^1S_0$ with $n' \leq n = 1, \ldots, 5$. The $1s$, $2s$, $3s$, $4s$ and $5s$ orbitals are simply taken as their Thomas-Fermi estimates. The density matrix eigenvectors are shown on Fig. 1 as given by `RDENSITY`. The dominant component of each eigenvector (printed as a column) is highlighted in red. Firstly the eigenvectors are shown in decreasing order of their corresponding eigenvalues. This sometimes leads to change in dominance, e.g. the eigenvector #3, corresponding to the $\widetilde{3}s$ natural orbital, has its largest component corresponding to the original $5s$ orbital. Finally, the eigenvectors are shown as sorted according to their dominant component, i.e., their dominant component is now on the diagonal and eigenvector #1 corresponds to the $\widetilde{1}s$ natural orbital, #2 to $\widetilde{2}s$, #3 to $\widetilde{3}s$ …, and so on. Note that if the CSF expansion is complete so that the total wave function is invariant under rotations of orbitals, the choice of the orbital labelling cannot affect the computed properties. Finally, the program deals with multiple levels, whether they have the same J-value or not. A radial density is computed for each level while the natural orbitals are computed as a statistical mixture over all levels. The latter is built from the following weighted sum

$$\overline{\rho}^{\kappa}_{n'n} = \frac{1}{\sum_i (2J_i + 1)} \sum_i (2J_i + 1)\, \rho^{\kappa}_{n'n}(\alpha_i J_i)\,, \tag{25}$$

where $\rho^{\kappa}_{n'n}(\alpha_i J_i)$ is the density matrix (21) for the state $\alpha_i J_i$. The final density matrix $\overline{\rho}^{\kappa}_{n'n}$ is then diagonalized and its eigenvectors are used to build the natural orbitals. Hence, only one natural orbital basis is constructed.

5. Applications and examples

Relativistic effects As a first example we computed the radial electron density distribution $D(r)$ of the ground state $[\mathrm{Rn}]5f^{14}6d^{10}7s^27p^6\ ^1S_0$ of neutral oganesson ($Z = 118$), the heaviest element recognised by IUPAC [40]. Large relativistic effects are already observed when comparing HF and DHF calculations in the single-configuration approximation. Figs. 2a and 2b display the corresponding radial electron density and its tail, respectively. The relativistic contraction of the most inner shells, identified by the principal quantum number n, is reproduced as in the work of Lackenby et al. [20], and the smoother relativistic tail of the radial density is in agreement with the original calculations using electron localization functions [22]. The normalisation property, $\int_0^\infty D_{\mathrm{Og}}(r)\, dr = 118$, is verified for both the relativistic and non-relativistic densities. The script `script_Og.sh` provided as a test-case for the present program computes the relativistic radial density of oganesson. The nuclear model used for oganesson is a Fermi distribution according to the description of finite-size nuclei within the GRASP2018 package. In the following, all nuclei are similarly described by a Fermi distribution. The execution of the test-case requires the prior installation of the GRASP2018 package. In Figs. 3a, 3b, 3c and 3d are displayed the radial density functions of the ground states of the heaviest noble gases, Kr ($Z = 36$), Xe ($Z = 54$), Rn ($Z = 86$) and Og ($Z = 118$). These figures illustrate the progressive increase of relativistic effects with the atomic number, i.e., the innermost shells are more and more contracted. The lightest of the four studied elements, krypton, shows almost no difference between the relativistic and non-relativistic electron densities.

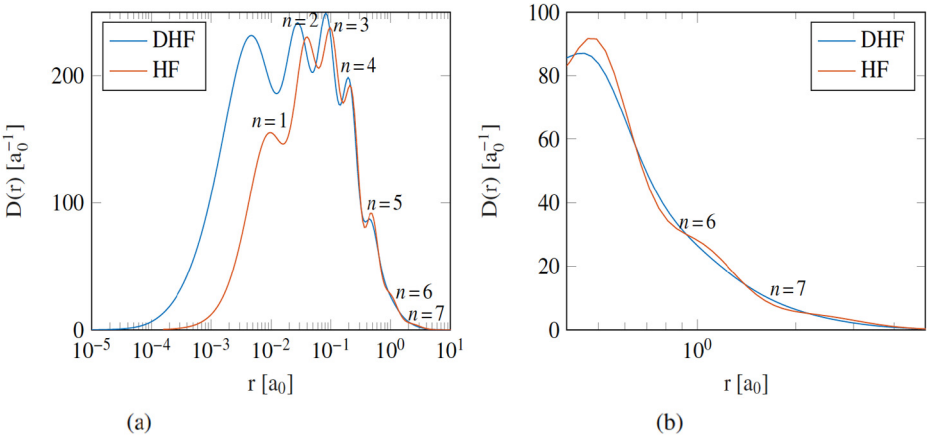

Fig. 2. Radial density distribution of the Og ($Z = 118$) atom in the Dirac-Hartree-Fock (relativistic) and Hartree-Fock (non-relativistic) approximations.

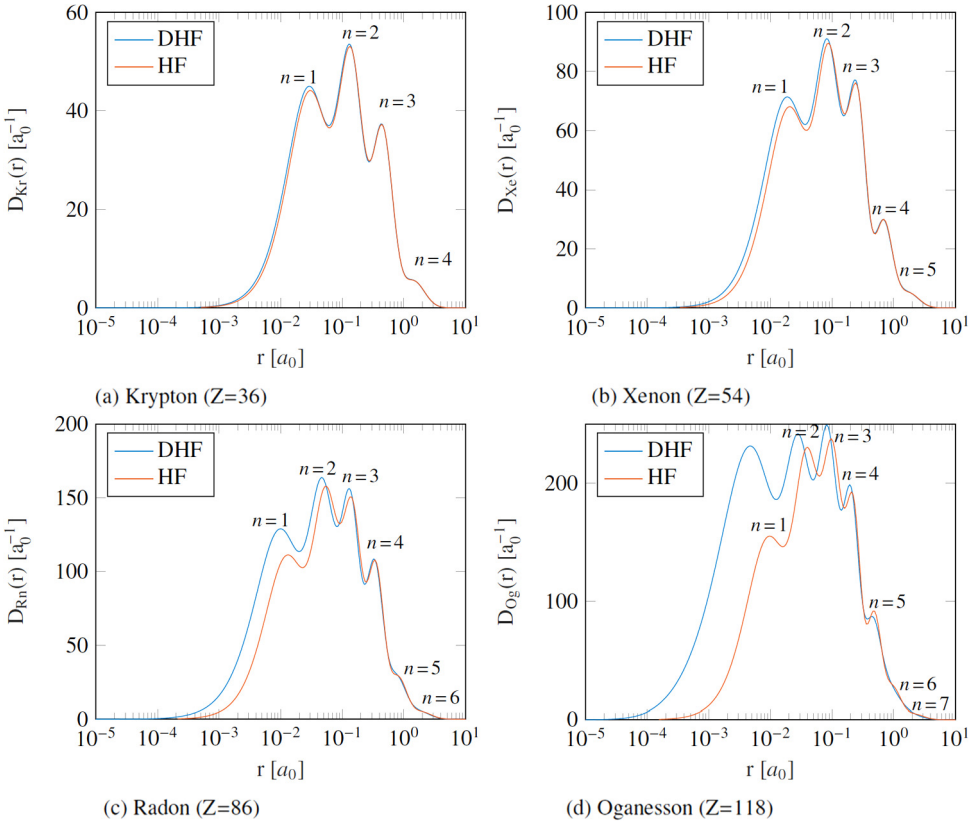

Fig. 3. Radial electron density distributions of the ground states of noble gases Kr, Xe, Rn and Og, calculated in the HF and DHF approximations.

Natural expansions The diagonalization of the density matrix (21) provides the natural-orbital basis, leading to an alternative representation of the wave function. Inspired by the non-relativistic work on beryllium [16], the relativistic natural-orbital expansion is presented for the Be ground state. The active space is built by allowing all single and double excitations from the $2s^2$ valence electron pair. Table 1 presents the mixing coefficients and the total binding energy using four different orbital bases. According to the expression of the density matrix (21), the transformation to the natural orbitals does not involve any radial integral and only depends on spin-angular coefficients and mixing coefficients. The NOs therefore reflect the structure of the active space, and the original orbital basis does not have to be optimal for the total binding energy. The first two orbital bases presented in Table 1 are generated using the Thomas-Fermi potential and their corresponding natural orbitals. The natural expansion reduces the number of CSFs, removing the contributions of the $1s^2 n\kappa\, n'\kappa\ \ ^1S_0$ configurations with $n \neq n'$. These corresponding zero mixing coefficients are counterbalanced by an increase in the weights of other configurations, in particular of the DHF CSF ($c_1 \leq \widetilde{c}_1$). The total energy is left unchanged by the transformation, as it is expected for complete active spaces [18]. The second test-case provided along with the present program reproduces the zero mixing coefficients appearing in the natural orbitals basis. As for the previous test-case, the execution of the script `script_TF.sh` requires the prior installation of the GRASP2018 package. A second set of calculations is performed using the same active space but optimising the orbital basis according to the variational MCDHF method [24], adopting a layer-by-layer optimisation strategy. The corresponding NOs are built. Similar observations as for the T-F basis can be made, i.e., CSFs of the kind $1s^2 n\kappa\, n'\kappa$ ($n' \neq n$) have their mixing coefficient reduced to zero and $c_1 \leq \widetilde{c}_1$. The total binding energy is still invariant with respect to the orbital transformation but is lower than the one obtained using the T-F orbital

Table 1
Mixing coefficients for the $n = 4$ active space expansion of the $1s^2 2s^2\ {}^1S_0$ ground state of Be, using four different orbital bases: the Thomas-Fermi (T-F) estimates and their corresponding natural orbitals (T-F/NO), and the MCDHF optimized orbitals and their corresponding (different) natural orbitals (MCDHF/NO).

CSF	T−F	T−F/NO	MCDHF	MCDHF/NO
1s (2) 2s (2)	0.940719	0.952668	0.952574	0.953379
1s (2) 2s (1) 3s (1)	−0.140880	0.000000	−0.037346	0.000000
1s (2) 2s (1) 4s (1)	−0.058189	0.000000	−0.013990	0.000000
1s (2) 2p (2)	0.246808	0.246873	0.243579	0.243601
1s (2) 2p-(2)	0.174525	0.174570	0.172267	0.172283
1s (2) 2p (1) 3p (1)	0.005658	0.000000	−0.003123	0.000000
1s (2) 2p (1) 4p (1)	0.000048	0.000000	−0.001022	0.000000
1s (2) 2p-(1) 3p-(1)	0.003964	0.000000	−0.002213	0.000000
1s (2) 2p-(1) 4p-(1)	0.000016	0.000000	−0.000721	0.000000
1s (2) 3s (2)	−0.016337	−0.031493	−0.039746	−0.040575
1s (2) 3s (1) 4s (1)	−0.010244	0.000000	0.003377	0.000000
1s (2) 3p (2)	0.000541	0.000692	0.004352	0.004404
1s (2) 3p-(2)	0.000380	0.000488	0.003084	0.003120
1s (2) 3p (1) 4p (1)	0.000471	0.000000	−0.000888	0.000000
1s (2) 3p-(1) 4p-(1)	0.000332	0.000000	−0.000627	0.000000
1s (2) 3d (2)	−0.001800	−0.002534	−0.013164	−0.013168
1s (2) 3d-(2)	−0.001470	−0.002069	−0.010746	−0.010749
1s (2) 3d (1) 4d (1)	−0.001638	0.000000	0.000288	0.000000
1s (2) 3d-(1) 4d-(1)	−0.001337	0.000000	0.000235	0.000000
1s (2) 4s (2)	−0.003215	−0.000008	−0.004974	−0.004950
1s (2) 4p (2)	0.000182	−0.000035	−0.001134	−0.001208
1s (2) 4p-(2)	0.000128	−0.000025	−0.000804	−0.000857
1s (2) 4d (2)	−0.000708	0.000026	−0.002818	−0.002814
1s (2) 4d-(2)	−0.000578	0.000022	−0.002299	−0.002296
1s (2) 4f (2)	−0.000020	−0.000020	0.004810	0.004810
1s (2) 4f-(2)	−0.000018	−0.000018	0.004165	0.004165
Energy (in E_h)	−14.6039671		−14.6218410	

basis, as it should be the case according to the variational principle. The reduction property of the active space is therefore independent of the choice of the original basis.

Electron correlation The radial density is helpful to visualize electron correlation in real space. The difference between the DHF density and the correlated density reveals radial changes induced by electron correlation. We take as an example the Ca^+ [Ar]$4p\ {}^2P^o_{1/2}$ excited state. Electron correlation is progressively included, following a layer by layer approach, in which only the last orbital per κ-symmetry is optimized. Core-valence correlation was included by allowing single and restricted double excitations from the $2s^2 2p^6 3s^2 3p^6$ core (at most one excitation from the core) but keeping the $1s$ shell closed. The radial density was computed after adding seven correlation layers. The difference between the correlated radial density $D^{\mathrm{CV}}_{1/2}(r)$ and the DHF radial density $D^{\mathrm{DHF}}_{1/2}(r)$ is displayed in Fig. 4. In the same plot, we show the radial density $D^{\mathrm{CV}}_{1/2}(r)$ to facilitate the analysis of the radial changes induced by electron correlation. The impact of electron correlation is most important in the outermost region, i.e. largest correlation effect in absolute value and low density value. Electron correlation has almost no influence closer to the nucleus, as expected since the $1s$ electrons are not involved in the correlation model. Finally, one should notice that the difference in the radial density is either positive or negative, but its integrated change is zero since $\int_0^\infty D(r)\,dr = N$ reflects the number of electrons. The radial density is therefore helpful to visualize the extra valence electron in a neutral/ion comparison, such as Ca/Ca^+. The difference in their radial density provides an efficient tool to visualize in space the electron density depletion associated with the ionization process, since $\int_0^\infty \left(D^{\mathrm{Ca}}(r) - D^{\mathrm{Ca}^+}(r)\right) dr = 1$.

Natural orbitals in hyperfine structure, field shift and transition data calculations The use of natural orbitals in atomic multiconfiguration variational methods, such as the MCDHF method, is rare. NOs were recently employed to estimate the hyperfine structure constants of Na and Na-like ions [18]. The transformation of the MCDHF orbitals to the NOs was shown to increase significantly the value of the magnetic dipole hyperfine constant of the Na ground state, leading to a much better agreement with the experimental value known with high accuracy. The increase of the magnetic dipole constant correlates with the contraction of the spectroscopic $3s$ orbital, as observed in earlier many-body perturbation theory calculations [41]. The influence of the NOs on other atomic properties is currently under investigations. Our two main goals are the evaluation of field shifts in Fr and transition rates of Na-like Si. Preliminary results are promising. The effect of the contraction of the spectroscopic valence orbital observed in the hyperfine structure calculations of Na is expected to play a comparable role for the field shift in Fr, due to its alkali-metal electronic structure and to the same one-electron character of the hyperfine structure and field shift operators. Coupled cluster calculations in Fr revealed similar effects using Brueckner orbitals [42]. The potential benefit of using NOs for computing transition rates is even less known due to the lack of studies. Preliminary results on Na-like Si, based on the large-scale calculations by Atalay et al. [43], indicate a decrease of the gauge discrepancy of transition rates for transitions involving high Rydberg states. Furthermore, we observe an unexpected larger stability of the Coulomb gauge relatively to the Babushkin one. This corroborates the conclusions of a recent MCDHF study of carbon ions [44] reporting a high sensitivity of radiative data to the orbital basis optimisation for transitions involving high Rydberg states.

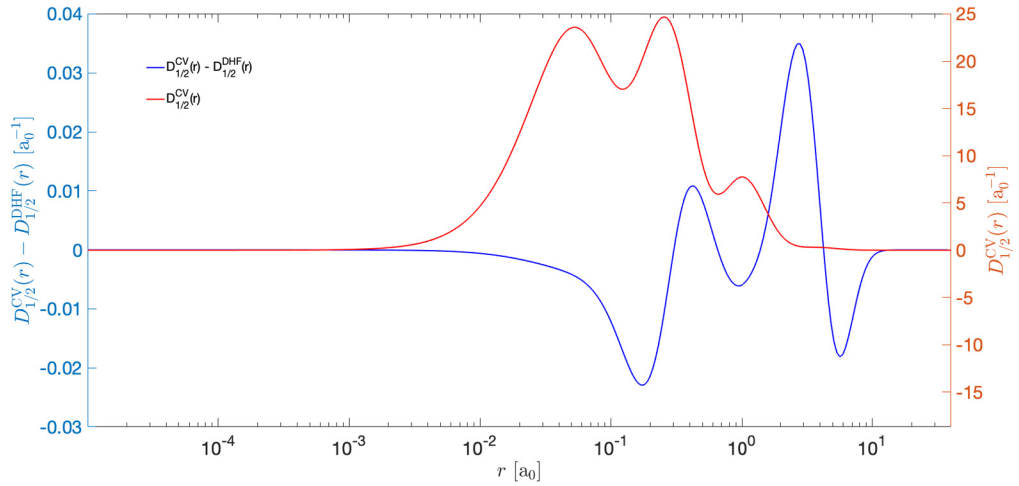

Fig. 4. Influence of electron correlation on the radial density distribution. In red, the radial density of the [Ar]$4p\ ^2P_{1/2}$ state of Ca^+ after including correlation. In blue, the difference between the correlated radial density and the DHF radial density.

6. Conclusions and outlook

We presented and described RDENSITY, a program to compute the radial electron density and the natural orbitals in the framework of the MCDHF/RCI method, as implemented in the GRASP2018 package. We illustrated the main features of this original module by considering relativistic effects, electron correlation and natural orbital expansions. The radial electron density picture provides a useful way to investigate electron correlation and relativistic effects on atomic systems. The advantages of the natural orbitals, often considered as a "by-product" of the evaluation of the electronic density, were demonstrated recently for the determination of the hyperfine structure of Na [18]. We hope that RDENSITY will be used by the atomic physics community as a complementary computational tool of the GRASP2018 package to further explore the use of NOs and to measure their efficiency in the estimation of various atomic properties using relativistic multiconfiguration variational wave functions.

GRASP is a package allowing the calculation of elaborate wave functions of many-electron atomic systems based on wave-function methods. The role of spherical symmetry is crucial in the sense that the variational principle is applied on symmetry-adapted wave functions, in contrary with other methods where the rotational symmetry is restored afterwards by projecting the deformed mean-field wave function on good total angular momentum, leading to "projection after variation" methods [45]. In the context of the relativistic description of field-free atoms, we therefore only consider the 1D *radial* electronic density that is obtained by averaging the density functions calculated with the $(2J+1)$ degenerate magnetic sublevels wave functions $\Psi_{\alpha JM_J}$. In density-functional approaches, building rules of the general 3D one- and two-particle density-matrix operators can be found [46]. It might be interesting to investigate this formalism to build the 3D atomic electronic density and natural orbitals when the rotational invariance is broken due to an external field [47] or to the chemical environment [48].

Declaration of competing interest

The authors declare that they have no known competing financial interests or personal relationships that could have appeared to influence the work reported in this paper.

Acknowledgements

MG acknowledges support from the FWO & FNRS Excellence of Science Programme (EOS-O022818F). SS is a FRIA grantee of the Fonds de la Recherche Scientifique—FNRS. JGL acknowledges the financial support by the National Natural Science Foundation of China (Grant No. 11874090).

References

[1] P. Löwdin, Phys. Rev. 97 (1955) 1474–1489.
[2] D. Feller, E. Davidson, J. Chem. Phys. 84 (1984) 1006–1017.
[3] D. Feller, E. Davidson, J. Chem. Phys. 88 (1988) 7581–7587.
[4] B. Engels, L.A. Eriksson, S. Lunell, Adv. Quantum Chem., Vol. 27, Academic Press, 1996, pp. 297–369.
[5] I. Lindgren, J. Lindgren, A.-M. Mårtensson, Z. Phys. A 279 (1976) 113–125.
[6] A.-M. Mårtensson-Pendrill, S. Salomonson, Phys. Rev. A 30 (2) (1984) 712–721.
[7] B. Engels, S.D. Peyerimhoff, E.R. Davidson, Mol. Phys. 62 (1987) 109–127.
[8] L. Bytautas, J. Ivanic, K. Ruedenberg, J. Chem. Phys. 119 (16) (2003) 8217–8224.
[9] P-O. Löwdin, H. Shull, Phys. Rev. 101 (1956) 1730–1739.
[10] C. Froese Fischer, The Hartree-Fock Method for Atoms. A Numerical Approach, John Wiley and Sons, New York, 1977.
[11] T.L. Gilbert, Phys. Rev. B 12 (1975) 2111–2120.
[12] M. Piris, Phys. Rev. Lett. 119 (2017) 063002.
[13] R. van Meer, O.V. Gritsenko, E.J. Baerends, J. Chem. Phys. 148 (10) (2018) 104102.
[14] F. Neese, F. Wennmohs, A. Hansen, J. Chem. Phys. 130 (2009) 114108.
[15] K.J.H. Giesbert, Chem. Phys. Lett. 591 (2014) 220–226.

[16] A. Borgoo, O. Scharf, G. Gaigalas, M. Godefroid, Comput. Phys. Commun. 181 (2010) 426–439.
[17] A. Borgoo, M. Godefroid, K. Sen, F. De Proft, P. Geerlings, Chem. Phys. Lett. 399 (2004) 363–367.
[18] S. Schiffmann, C. Froese Fischer, J. Ekman, M. Godefroid, P. Jönsson, Phys. Rev. A 101 (2020) 062510.
[19] I.P. Grant, Relativistic Quantum Theory of Atoms and Molecules. Theory and Computation, Atomic, Optical and Plasma Physics Series, Springer, New York, 2007.
[20] B.G.C. Lackenby, V.A. Dzuba, V.V. Flambaum, Phys. Rev. A 98 (2018) 042512.
[21] V. Pershina, Nucl. Phys. 944 (2015) 578–613.
[22] P. Jerabek, B. Schuetrumpf, P. Schwerdtfeger, W. Nazarewicz, Phys. Rev. Lett. 120 (2018) 053001.
[23] A. Almoukhalalati, S. Knecht, H.J.A. Jensen, K.G. Dyall, T. Saue, J. Chem. Phys. 145 (7) (2016) 074104.
[24] C. Froese Fischer, M. Godefroid, T. Brage, P. Jönsson, G. Gaigalas, J. Phys. B, At. Mol. Opt. Phys. 49 (18) (2016) 182004.
[25] B. Judd, Second Quantization and Atomic Spectroscopy, The Johns Hopkins Press, Baltimore, MD, 1967.
[26] B. Judd, in: G. Drake (Ed.), Second Quantization, in Springer Handbook of Atomic, Molecular, and Optical Physics, Springer New York, New York, NY, 2006, pp. 115–121.
[27] A.R. Edmonds, Angular Momentum in Quantum Mechanics, Princeton University Press, New Jersey, 1957.
[28] J. Olsen, M. Godefroid, P. Jönsson, P.-A. Malmqvist, C. Froese Fischer, Phys. Rev. E 52 (1995) 4499–4508.
[29] R. McWeeny, Methods of Molecular Quantum Mechanics, Academic Press, London, 1992.
[30] Z.B. Rudzikas, Theoretical Atomic Spectroscopy, Cambridge University Press, Cambridge, 1997.
[31] G. Gaigalas, S. Fritzsche, I. Grant, Comput. Phys. Commun. 139 (2001) 263–278.
[32] G. Gaigalas, Z. Rudzikas, J. Phys. B, At. Mol. Opt. Phys. 29 (18) (1996) 3303–3318.
[33] G. Gaigalas, S. Fritzsche, Comput. Phys. Commun. 267 (2021) 108086.
[34] G. Gaigalas, Z. Rudzikas, C. Froese Fischer, J. Phys. B, At. Mol. Opt. Phys. 30 (18) (1997) 3748–3771.
[35] C. Froese Fischer, G. Gaigalas, P. Jönsson, J. Bieroń, Comput. Phys. Commun. 237 (2019) 184–187.
[36] P. Jönsson, G. Gaigalas, J. Bieroń, C. Froese Fischer, I. Grant, Comput. Phys. Commun. 184 (2013) 2197.
[37] J. Ekman, P. Jönsson, M. Godefroid, C. Nazé, G. Gaigalas, J. Bieroń, Comput. Phys. Commun. 235 (2019) 433–446.
[38] J. Bieroń, C. Froese Fischer, G. Gaigalas, I. Grant, P. Jönsson, A practical guide to Grasp 2018, https://github.com/compas/grasp2018/releases/download/2018-12-03/GRASP2018-manual.pdf.
[39] E. Anderson, Z. Bai, C. Bischof, S. Blackford, J. Demmel, J. Dongarra, J. Du Croz, A. Greenbaum, S. Hammarling, A. McKenney, D. Sorensen, LAPACK Users Guide, Society for Industrial and Applied Mathematics, Philadelphia, PA, 1999.
[40] J.H. Hamilton, S. Hofmann, Y.T. Oganessian, Annu. Rev. Nucl. Part. Sci. 63 (1) (2013) 383–405.
[41] I. Lindgren, J. Lindgren, A.-M. Pendrill, Z. Phys. A 279 (1976) 113–125.
[42] A.-M. Mårtensson-Pendrill, Mol. Phys. 98 (16) (2000) 1201–1204.
[43] B. Atalay, T. Brage, P. Jönsson, H. Hartman, Astron. Astrophys. 631 (2019) A29.
[44] A. Papoulia, J. Ekman, G. Gaigalas, M. Godefroid, S. Gustafsson, H. Hartman, W. Li, L. Radžiūtė, P. Rynkun, S. Schiffmann, K. Wang, P. Jönsson, Atoms 7 (4) (2019) 106.
[45] M. Bender, P.-H. Heenen, P.-G. Reinhard, Rev. Mod. Phys. 75 (2003) 121.
[46] J. Toulouse, SciPost Chem. 1 (2021) 2.
[47] W. Li, J. Grumer, T. Brage, P. Jönsson, Comput. Phys. Commun. 253 (2020) 107211.
[48] G. Gaigalas, D. Kato, Comput. Phys. Commun. 261 (2021) 107772.